# Preparation of Cellulose Nanocrystals Using Highly Recyclable Organic Acid Treated Softwood Pulp

Songlin Wang,[a,b,*] Fei Wang,[a] Zongjia Song,[a] Xiaoming Song,[a] Xuxu Yang,[a] and Qian Wang [a]

Cellulose nanocrystals (CNC) were successfully obtained from softwood pulp by p-toluenesulfonic acid (p-TsOH) hydrolysis under the treatment of p-TsOH mass concentration of 60%, temperature of 70 °C, reaction time of 4 h, and pulp to solution ratio of 1:20 (g / mL). Zeta potential and dynamic light scattering (DLS), scanning electron microscopy (SEM), X-ray diffraction (XRD), Fourier-transform infrared spectroscopy (FTIR), X-ray photoelectron spectroscopy (XPS), and thermogravimetric analysis (TGA) were used to characterize the physical-chemical properties of the CNC. Under these conditions, the CNC exhibited good thermal stability in the suspension with a high crystallinity index of 90.1%. The CNC had an average diameter of 4.87 nm and average length 175.5 nm with no undesired elemental contamination. The degradation temperature of the CNC was relatively high at 310 °C. Moreover, p-TsOH was recovered by crystallization technology, and the recovery rate was over 70%, providing an environmentally friendly way for the development of biomass materials.

*Keyword: Softwood pulp; p-TsOH hydrolysis; Cellulose nanocrystals; Acid recovery*

*Contact information: a: College of Marine Science and Biological Engineering, Shandong Provincial Key Laboratory of Biochemical Engineering, Qingdao University of Science & Technology, Qingdao, Shandong 266042 China; b: Key Laboratory of Pulp and Paper Science & Technology of Ministry of Education/Shandong Province, Qilu University of Technology, Jinan, Shandong 250353 China;*
** Corresponding author: wangsongl@126.com*

## INTRODUCTION

Cellulose is the most abundant renewable natural polymer resource, with an annual production of 14 to 20 billion tons (Lima and Borsali 2004; Habibi *et al*. 2010). Cellulose is widely distributed in higher plants, algae, fungi, bacteria, and some lower animals. Regardless of the source, the structure of cellulose is shown in Fig. 1. The basic unit is the D-pyranose-glucose group, which is a linear polymer linked by β-(1,4)-glycosidic bonds (Brinchi *et al*. 2013). Compared with synthetic polymer materials, cellulose has advantages of being renewable, degradable, non-toxic, and non-polluting. Cellulose is widely available at a low cost and, therefore, is an indispensable resource for society.

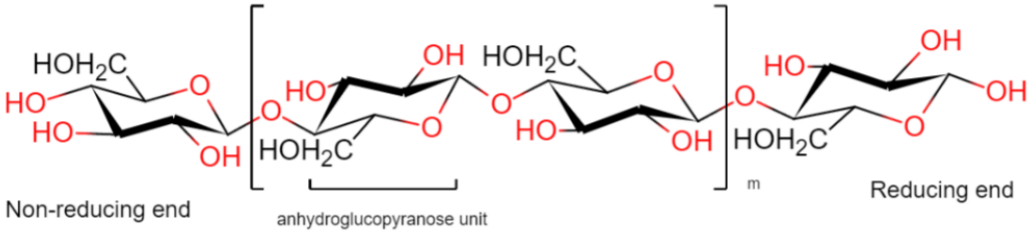


**Fig. 1.** Chemical structure of cellulose

The geometrical size and morphology of cellulose has different effects on its utilization. In general, plant-derived nanocelluloses can be divided into two categories: cellulose nanofibers (CNF) and cellulose nanocrystals (CNC). CNC, with a diameter of 5 to 20 nm and a length of several hundred nanometers, have many excellent properties such as high surface area (Stelte and Sanadi 2009; Sandeep *et al*. 2014), high mechanical strength and stiffness, high modulus, high crystallinity, biodegradability, and good hydrophilicity. It can be used as a functional material in gels (Aulin *et al*. 2010; Dong *et al*. 2013; Zhang *et al*. 2018), optoelectronics (Miettunen *et al*. 2014; Zu *et al*. 2016; Xing *et al*. 2018), adsorbent materials (Fernandes *et al*. 2013; Lin and Dufresne 2014; Sol 2016; Seabra *et al*. 2017), and medical materials (Carlsson *et al.* 2012; Liu *et al.* 2015; Karim *et al.* 2016; Mishra *et al*. 2018). CNC can also be used as a nanofiller in film materials (Stelte and Sanadi 2009; Belbekhouche *et al*. 2011; Herrera *et al*. 2014; Sandeep *et al*. 2014; Guo *et al*. 2018) or as a reinforcing agent in composite materials (Samir *et al*. Dufresne 2005; Choi and Simonsen 2006; Chang *et al*. 2010; Dufresne 2013; Oksman *et al*. 2016). In recent years, the application of CNC has aroused widespread concern among researchers.

Most preparation methods for CNC include an acid hydrolysis method and an enzymatic method (Teixeira *et al*. 2015), in which the sulfuric acid method (Coelho *et al*. 2018; Theivasanthi *et al*. 2018; Maciel *et al*. 2019) is the most widely used. Acid hydrolysis releases a single crystallite by breaking the β-glycosidic bond of the amorphous region of cellulose, while the crystalline region maintains its integrity, producing CNC with high crystallinity of rod-like structure. The geometry of the CNC depends on the cellulose source and the acid hydrolysis treatment. The cellulose hydrolyzed is used to obtain CNC, and the hydroxyl groups on the cellulose surface is partially esterified to produce a negatively charged sulfate group. This helps the CNC suspension to have good dispersability (Tingaut *et al*. 2012). However, the sulfate group in the crystal reduces the thermal stability of the nanocellulose (Roman and Winter 2004). In addition, sulfuric acid is highly corrosive to equipment, and the recovery of sulfuric acid and the treatment of sulfate is still a huge challenge. Moreover, the recovery of sulfuric acid and the treatment of sulfate is still a great challenge. Compared with the inorganic acid hydrolysis method, the organic acid hydrolysis method has milder reaction conditions, less corrosiveness to equipment, relatively easier recovery of the organic acid, and environmentally friendly character.

Dicarboxylic acids have been used to prepare CNC (Bian *et al*. 2017). Carboxylated CNC has good thermal stability and solves the problem of acid recovery. However, as an organic acid, maleic acid is weak in acidity and insufficient degradation of cellulose results in low yield. The endoglucanase/β-glucosidase has the function of catalyzing the β-glycosidic bond of the amorphous region of cellulose to promote hydrolysis, and it can advantageously adjust the size of the CNC, which the reaction treatment was mild and can protect the cellulose from severe degradation. But since CNC obtained by enzymatic hydrolysis process does not have a surface negative charge, this results in poor stability of the suspension and longer enzymatic reaction time. Chen *et al.* (2016) used four organic acids (oxalic acid, maleic acid, p-toluenesulfonic acid, benzenesulfonic acid) to prepare CNC (Chen *et al.* 2016), but the relevant content of p-toluenesulfonic acid (p-TsOH) was very small. In this study, the preparation of CNC from p-toluenesulfonic acid was considered in depth.

p-TsOH can be used for delignification and efficiently recovered by crystallization technology (Bian *et al*. 2017; Chen *et al*. 2017). Research on preparing CNC by hydrolysis with p-TsOH is very rare. In this study, CNC was successfully prepared by hydrolysis of a

strong organic acid p-TsOH. Cellulose nanocrystals are characterized by DLS and zeta potentials, Zeta potential and dynamic light scattering (DLS), scanning electron microscopy (SEM), X-ray diffraction (XRD), Fourier-transform infrared spectroscopy (FTIR), X-ray photoelectron spectroscopy (XPS), and thermogravimetric analysis (TGA) to evaluate the physicochemical properties of CNC. The relatively low water solubility of p-TsOH, can be efficiently recovered by cooling the concentrated spent acid solution using crystallization technology.

## EXPERIMENTAL

### Materials

The p-TsOH was purchased from Tianjin Damao Chemical Reagent Factory (Tianjin, China), which was analytical grade and no further purification was required. The pulp board that was prepared from softwood was provided free of charge by Shandong Chenming Paper Group Co., Ltd. (Shandong, China).

### Methods

*Preparation of CNC*

A scheme for the preparation of CNC is shown in Fig. 2. The p-TsOH solution of desired mass concentration (50% to 80%) was prepared by adding the required amounts of p-TsOH and 50 mL deionized water into a 150 mL flask. One hundred mL of acid solution and 5 g (oven-dry weight) of pulverized pulp (the solid-liquid ratio used in all treatments was 1:20 (g / mL) was heated in a three-necked flask to 70 °C and was treated for 4 h with continuous stirring at 200 rpm.

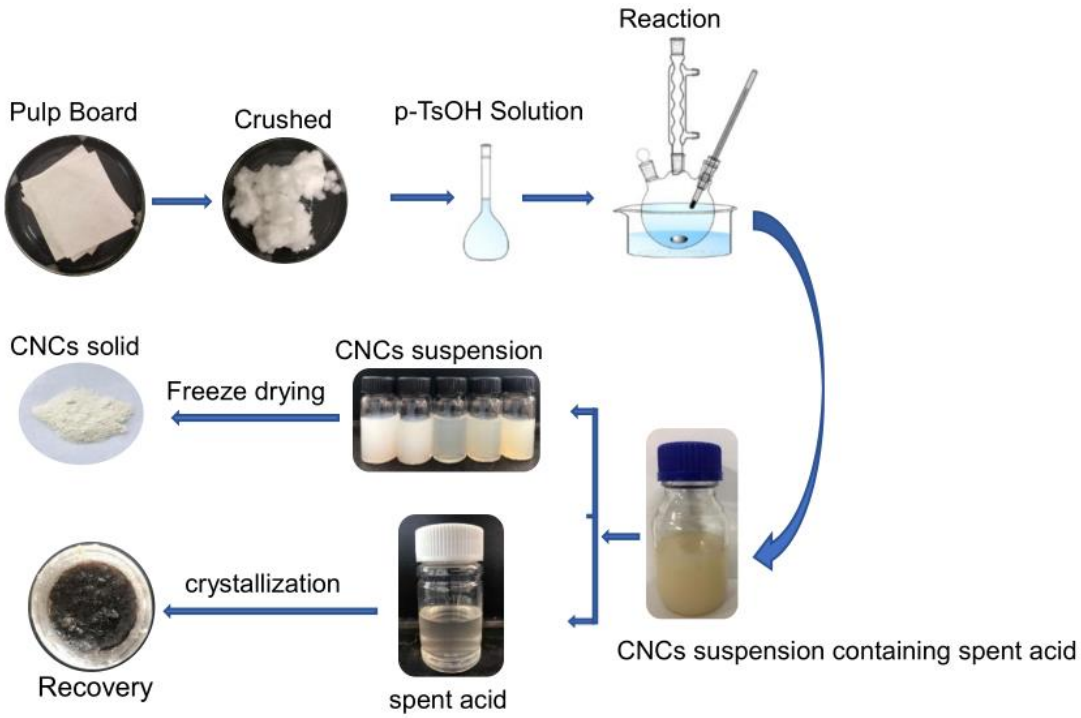


**Fig. 2.** A schematic process flow diagram illustrating the preparation of CNC by catalytic hydrolysis of p-TsOH

The reaction was stopped by adding 100 mL of deionized water (25 °C) into the flask. The sample obtained by acid hydrolysis was repeatedly washed by centrifugation (4000 rpm, 10 minutes) to remove the spent acid until the suspension was neutral. Then centrifugation was continued to separate the CNC (supernatant) from the hydrolyzed macromolecular cellulose (precipitation). The obtained suspension of CNC was freeze-dried to obtain a solid of CNC.

*Recovery of p-toluenesulfonic acid*

The spent acid was recovered by crystallization. The spent acid was concentrated using a rotary evaporator (RE-52CS, Shanghai, China) under the conditions of a vacuum of -0.1 MPa and a temperature of 50 °C. The concentrated spent acid solution was transferred to a beaker and cooled at a rate of 1 °C/min. The crystal began to precipitate when the temperature reached 19.4 °C. It was allowed to stand at this temperature for a period of time until the crystallization process had been completed. The precipitated crystals were separated from the spent acid solution by vacuum filtration, and the crystal mass was weighed to calculate the recovery of p-TsOH.

## Characterization

*Dynamically scattered light (DLS) and zeta potential*

The CNC suspension was further dispersed by ultrasonic treatment and placed in an equipped colorimetric cuvette. The size and zeta potential of the CNC was measured using a particle size analyzer (Malvern Zetasizer Nano series, Malvern, UK). The measuring parameters are set on the computer, in which the material is protein, the dispersing medium is water, and the equilibrium time is 120 s. The sample was cycled 3 times at 25 °C to obtain the average size and zeta potential of the sample.

*Scanning electron microscope (SEM)*

The cellulose of the pulp board and the obtained CNC image was observed and recorded using a scanning electron microscope (SEM) (JSM-6380, Jeol, Beijing, China) in order to analyze the morphology. All SEM samples mounted on a conductive aluminum plate were sputter coated with gold (Hitachi E-1010 Ion Sputtering System, Tokyo, Japan) for 90 s to provide sufficient conductivity under vacuum. At a current intensity of 1 to 2 mA and an accelerating voltage of 8 kV, the sample was imaged at a magnification of 140000.

*Transmission electron microscope (TEM)*

Ten μL of the CNC suspension was deposited on a discharged carbon coated transmission electron microscope (TEM) grid, and excess liquid was absorbed using filter paper after 2 min. The sample was stained with 2% phosphotungstic acid solution; then excess dye solution was removed using filter paper. The sample was dried at room temperature and observed using a transmission electron microscope (JEM-2100PLUS, Japan JEOL Company, Beijing, China) at an acceleration voltage of 200 kV.

*X-ray diffraction (XRD)*

Diffraction patterns of all the samples was obtained by an X-ray diffractometer (D/max-2500; Japan Science Co., Shanghai, China), operating at 40 kV, 30 mA, and CuKa radiation ($I$ = 0.154 nm). The sample was ground into a powder and spread on a sample plate, then gently pressed with a cover glass to scan the sample from 5° to 60° ($2\theta$) at a rate

of 5°/min. The interplanar spacing of cellulose was calculated according to the Bragg's Law, and crystallinity index (CrI) was calculated according to Segal's empirical method (Segal *et al*. 1959),

$$2d \sin\theta = n\lambda \quad (1)$$

where d is the interplanar spacing, $\theta$ is the Bragg angle, and $\lambda$ is the X-ray wavelength.

$$CrI = \frac{I_{002} - I_{am}}{I_{002}} \times 100 \quad (2)$$

In Eq. 2, $I_{002}$ is the maximum intensity of diffraction of the lattice peak $2\theta$ = 22° to 23°, and $I_{am}$ is the minimum intensity of diffraction of the lattice peak at $2\theta$ between 18° and 19°.

*Fourier transform infrared spectroscopy (FTIR)*

The lyophilized CNC was analyzed for its chemical structure by Fourier transform infrared spectroscopy (FTIR) (VECTOR22; Germany Brooke Co., Ettlingen, Germany). Two mg of each sample was ground into a powder, and spectra were obtained at a resolution of 4 $cm^{-1}$ in the range of 4000 to 450 $cm^{-1}$ and averaged from 8 scans in transmission mode.

*X-ray photoelectron spectroscopy (XPS)*

The surface chemical changes of the CNC were analyzed by X-ray photoelectron spectroscopy (XPS) (ESCALAB Xi+ spectrometer, Thermo Fisher Scientific, Shanghai, China), in which the aluminum anode was operated at 150 W, and a high-resolution spectrum was obtained by energy using a 0.1 eV step and a 50 eV analyzer to obtain a binding spectrum of carbon and oxygen.

*Thermogravimetric Analysis (TGA)*

The thermal stability of pulp fibrils and cellulose nanocrystals was analyzed by thermogravimetric analyzers (TAQ-500; Shimadzu Co., Kyoto, Japan). All samples were heated from 25 °C to 800 °C at a rate of 10 °C/min under a nitrogen atmosphere (30 mL/min).

## RESULTS AND DISCUSSION

Cellulose nanocrystals were successfully obtained by hydrolysis of p-TsOH under different concentrations, temperatures, and times. The yield of CNC and the content of degradation products in the spent acid were determined. To facilitate discussion, PxTytz indicated a mass concentration of x %, a reaction temperature of y °C, and a reaction time of z hours. As shown in Table 1, the yield of the CNC gradually increased as the concentration and/or temperature and/or time increases. This indicates that in the case of relatively harsh reaction conditions, the cellulose chain was sheared to a small size, and the degradation of cellulose was also aggravated. The yield of CNC under the treatment of P60T70t7 was the largest. Bian *et al*. (2017) used a dicarboxylic acid to produce nanocellulose. The yield was low at only a few percent, since maleic acid is a weak acid and incapable of sufficiently depolymerizing chemical pulp fibers. However, the p-TsOH used in this article is a strong acid which can fully depolymerize cellulose.

**Table 1.** Yield of CNC and Content of Degradation Products under Different Treatment

| | Yield (%) | Average Zeta (mV) | Furfural (mg/mL) |
|---|---|---|---|
| P50T50t4 | 5.21 | -11.8 | 0.5281 |
| P50T70t4 | 9.86 | -13.3 | 1.583 |
| P60T70t4 | 15.81 | -26.5 | 5.231 |
| P70T70t4 | 16.40 | -21.5 | 5.367 |
| P80T70t4 | 16.97 | -18.0 | 6.130 |
| P60T70t2 | 9.32 | -18.5 | 2.753 |
| P60T70t3 | 10.79 | -20.4 | 5.766 |
| P60T70t5 | 21.5 | -17.3 | 5.890 |
| P60T70t6 | 35.3 | -20.0 | 7.409 |
| P60T70t7 | 40.1 | -17.5 | 13.859 |
| P60T50t4 | 8.05 | -19.4 | 3.3347 |
| P60T60t4 | 9.13 | -21.2 | 4.252 |
| P60T80t4 | 16.42 | -13.1 | 6.982 |

Note: For convenience of expression, PxTytz indicated a mass concentration of x %, a reaction temperature of y °C, and a reaction time of z hours.

Different hydrolysis treatments exhibit different colours in CNC suspensions. The color arises because conjugated unsaturated structure carbonyl groups are produced, and these are chromophores (Yatagai and Zeronian 1994; Łojewska *et al.* 2007). The color of CNC gradually deepened as the concentration and time increased, as shown in Fig. 3. The change of color indicates that the degradation of cellulose is aggravated (Heggset *et al.* 2017; Coelho *et al.* 2018). After termination of the reaction, the color of the product was as shown in Fig. 3(a). Under milder hydrolysis treatments, the pale-yellow material of the product can be removed by sonication and multiple centrifugation cycles to obtain a bluish colloidal suspension. Cellulose was degraded to produce substances such as furfural. Furfural in the spent acid can be quantified by a UV spectrophotometer (TU-1810, Beijing General Instruments Co., Ltd. Beijing, China) with wavelengths of 284 nm (furfural). As shown in Table 1, the content of furfural in the spent acid was under more severe reaction conditions, indicating increased degradation of cellulose. As shown in Fig. 3(b), the color of the CNC suspension darkened, so the reaction temperature, concentration, and time should be controlled to prevent excessive degradation. Moreover, the spent acid was recovered by crystallization technology, and the recovery rate reached 71.8%.

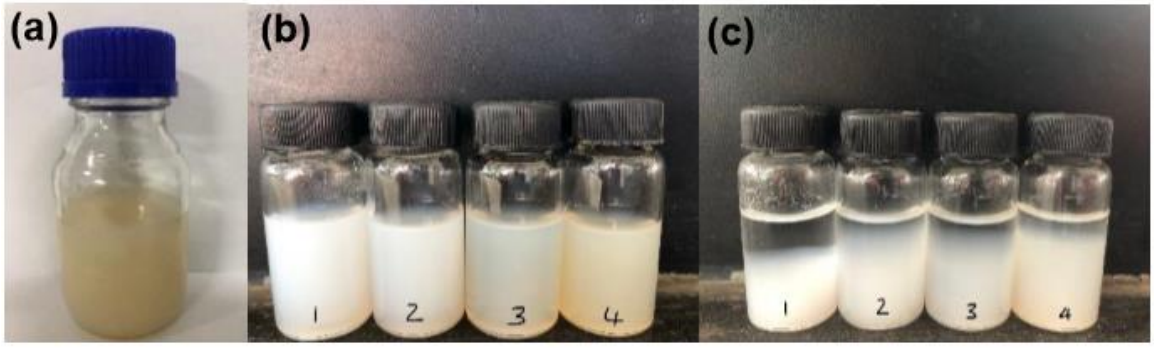


**Fig. 3.** CNC prepared under different hydrolysis conditions (where 1 is P50T50t4, 2 is P60T70t4, 3 is P70T70t4, 4 is P60T70t7)

As shown in Fig. 3(c), noticeable stratification occurred in suspension of P50T50t4 after about 40 days, while weak stratification occurred in suspension of P60T70t4, P70T70t4, and P60T70t7. This phenomenon can be further explained by the zeta potential (ζ). For systems with negative power, the stability of the system is better under a larger value of ζ. As shown in Table 1, the zeta potential of CNC ranged from -26.5 mV to -11.8 mV. P60T70t4 had the largest absolute value of zeta potential, and the best stability of CNC suspension. With a zeta potential above -25 mV, the suspension had good stability (Mirhosseini *et al*. 2008; Pereira *et al*. 2014). The hydrolysis process described herein was superior to the hydrochloric acid hydrolysis process in terms of suspension stability. The zeta potential of hydrochloric acid was -16.9 mV to -12.2 mV (Yu *et al*. 2013). However, compared with sulfuric acid and dicarboxylic acid hydrolysis, the suspension stability was relatively poor. The average potential of CNC prepared by sulfuric acid hydrolysis was above -40 mV, and the average potential of CNC obtained by hydrolysis of dicarboxylic acid was -30.9 mV to -46.8 mV (Morais *et al*. 2013; Tian *et al*. 2016; Bian *et al*. 2017).

## Morphologies of CNC (DLS, SEM, and TEM)

The morphologies of the CNC are important for its potential applications. Therefore, DLS, SEM, and TEM analyses of CNC were carried out to obtain the particle size distribution of CNC, and the microscopic morphology of CNC was observed. In Fig. 4, as the hydrolysis conditions became harsh, the particle size distribution of CNC moved toward a small size, probably because the β-glycosidic bond in cellulose broke and the long molecular chains of cellulose became short, which demonstrates that cellulose hydrolysis became more serious.

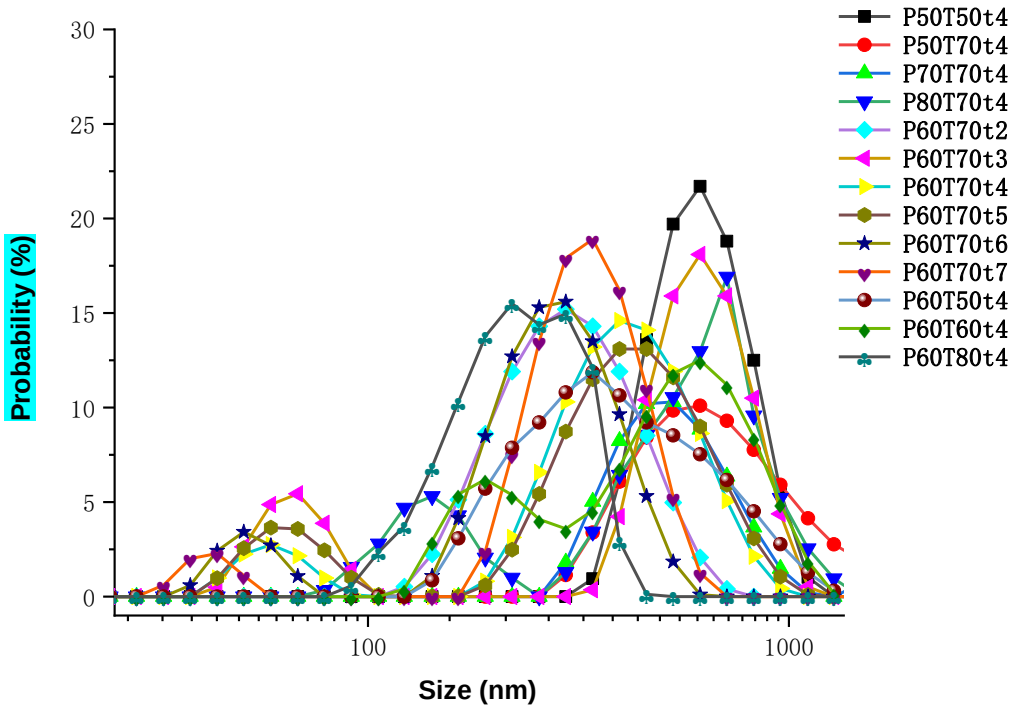


**Fig. 4.** Size distribution of CNC under different process conditions

The shape of the CNC can be observed in Fig. 5(a,b). The rod-shaped and interwoven network structure made the CNC more flexible and mechanically strong (Liu *et al*. 2016). This was an important feature of CNC as a reinforcing agent in composite materials (Xu *et al*. 2013). The CNC underwent self-aggregation and self-assembly during the freeze-drying process, forming large-size cellulose by hydrogen bonding in the lateral and longitudinal directions. Moreover, the use of SEM for inspection required a gold spray operation, which also increased the size of the CNC. The resolution of the TEM is larger than that of the SEM, and the measurement does not need to require the gold-plating operation. It can better observe the true shape of the numerical control system and the size distribution of the CNC measured from the TEM photograph.

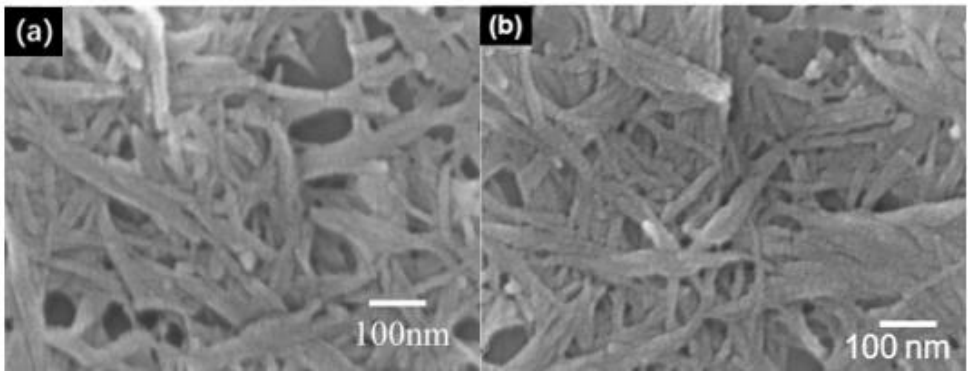


**Fig. 5.** SEM photographs of CNC obtained under P60T70t4(a) and P70T70t4(b)

The TEM image is shown in Fig. 6. The approximate contour of the intertwined CNC whiskers can be clearly seen, and the overlapped results in most CNC longitudinal and lateral dimensions are difficult to measure. Some fiber bundles with clear ends and lateral dimensions were selected for measurement.

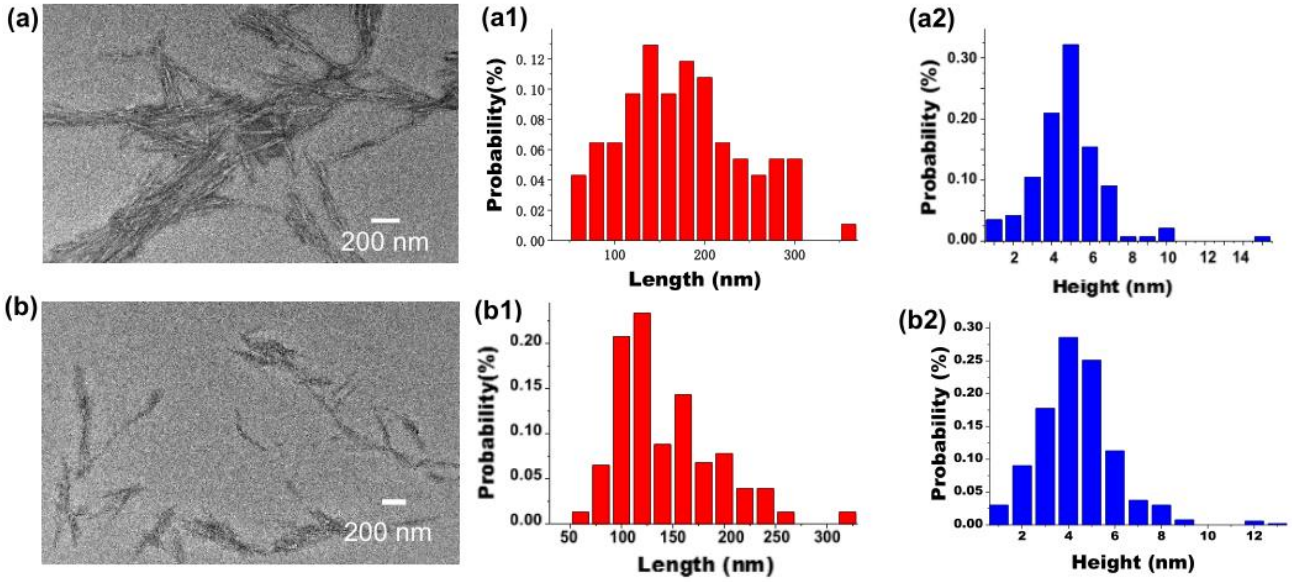


**Fig. 6.** TEM image and longitudinal and lateral size distribution of CNC prepared under different hydrolysis conditions (where a is P60T70t4 and b is P60T70t7, whereas a1, a2, b1, and b2 are the length and height of the CNC, respectively.)

The size and statistics of 120 sets of nanocellulose were measured here, and the size of CNC was roughly estimated. In the histograms a1 and a2 (Fig. 6), the average length and average diameter of the statistical CNC of P60T70t4 were 175.48 nm (range from 60 nm to 300 nm) and 4.87 nm (range was 5 ± 4 nm), respectively, and the corresponding average aspect ratio was 36.03 (range was 38 ± 12). In the histograms b1 and b2, the average length and average diameter of the statistical CNC of P60T70t7 were 143.2 nm (range from 60 nm to 200 nm) and 4.48 nm (range was 4.5 ± 3.5 nm), respectively, and the corresponding average aspect ratio was 31.96 (range was 30 ± 11). The harsher hydrolysis produced a shorter length of CNC, as previously noted (Elazzouzi-Hafraoui *et al*. 2008; Martínez-Sanz and Lagaron 2011). Due to its small diameter and large aspect ratio, CNC particles have been used in polymer nanocomposites to provide better mechanical properties (Grunert and Winter 2000; Orts *et al.* 2005; Santos *et al.* 2016; Nadir and Stephen 2017). And CNC particles having a large aspect ratio, when used as a nano-filler, have shown superior enhancement of properties (Mounika and Ravindra 2015).

## X-ray Diffraction (XRD)

Crystallinity is a major factor affecting the mechanical properties of materials. The crystallinity of the CNC can be varied by controlling the temperature, time, and concentration of the hydrolysis. The X-ray diffraction patterns of the CNC obtained under different conditions are shown in Fig. 7. Strong diffraction peaks appeared at 14.8°, 16.3°, and 22.5°, respectively, and weak diffraction peaks appeared at 34.3°, corresponding to four crystal faces of $1\bar{1}0$, 110, 002 and 040, respectively (Yu *et al*. 2013; Theivasanthi *et al*. 2018; Xing *et al*. 2018). The four crystal faces are characteristic peaks of typical natural cellulose, indicating that acid hydrolysis did not alter the cellulose form. However, the diffraction peak of the CNC controller deviated from the diffraction peak of the original cellulose. The Bragg angle of the CNC controller was slightly smaller than the Bragg angle of the material. According to the Bragg formula, $2d \sin \theta = n\lambda$, the surface distance $d$ of the crystal unit of the CNC was increased. This phenomenon can be attributed to the change in the size of the cellulose, resulting in different long-range compressive forces of the crystal and the unit cell (French 2014; Coelho *et al.* 2018).

Generally, the larger the full width at half maximum of the diffraction peak is, the smaller the size of the cellulose is (Yu *et al.* 2013; Xing *et al.* 2018). At $2\theta = 22.4°$, the full width at half maximum of the crystal diffraction peaks of P60T70t4, P70T70t4, and P60T70t7 increased sequentially, indicating that the size of the CNC decreased relatively with increasing concentration and/or reaction time, further confirming the results of DLS. In the X-ray diffraction pattern, the extreme values around 22° and 18° represented the crystalline and amorphous regions in the cellulose, respectively (French 2014; Xing *et al.* 2018). The peak changes at these two points can show changes in the crystal and amorphous regions of the CNC. At the peak of 18°, the crystal peaks of P60T70t4, P70T70t4, and P60T70t7 were weaker than the raw materials, indicating that p-TsOH can act on the amorphous region, and the amorphous region content of cellulose is decreased. At 22.4°, the crystal peak intensities of P60T70t4, P70T70t4, and P60T70t7 first increased and then decreased, indicating that the relative content of the crystallization zone decreased with vigorous hydrolysis. According to Siegel's empirical method, the crystallinity of the raw materials and the CNC obtained under the conditions of P60T70t4, P70T70t4, and P60T70t7 were 78.9%, 89.9%, 90.1%, and 82.6%, respectively. The change in crystallinity indicated that p-TsOH preferentially acted on the amorphous region under mild reaction conditions, retaining the crystalline region, and obtaining high crystallinity CNC.

However, as the reaction time, acid concentration, and temperature were increased, acid hydrolysis became intense, attacking the crystalline zone, destroying hydrogen bonds, and producing more disordered domains in the cellulose, resulting in a decrease in crystallinity. The change in crystallinity is consistent with the literature (Chen *et al*. 2015; Xing *et al.* 2018).

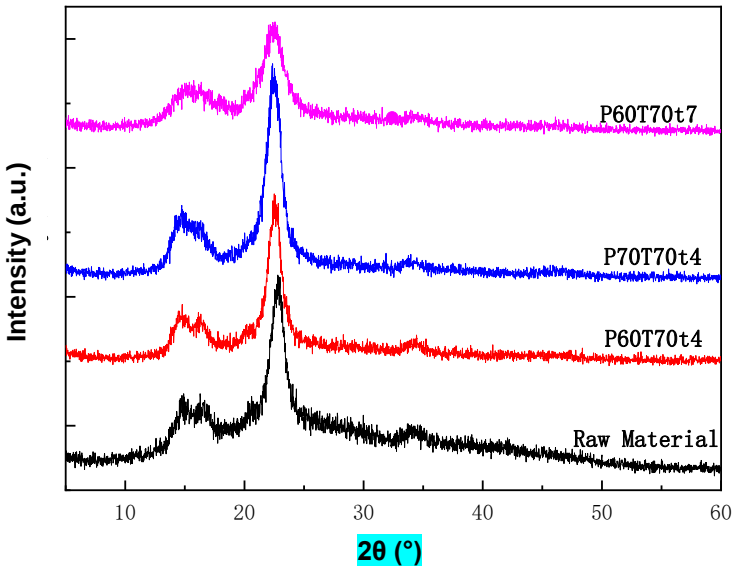


**Fig. 7.** X-ray diffraction pattern of CNC prepared under different hydrolysis treatments

## FTIR Analysis

The infrared spectra of the softwood pulp board and CNC are shown in Fig. 8. The infrared spectrum of the CNC prepared by hydrolysis did not show new peaks, indicating that the p-TsOH hydrolysis did not produce any new functional groups. The wavelengths of several samples mainly appeared in the ranges of 3700 to 2600 $cm^{-1}$ and 800 to 1700 $cm^{-1}$. The bands at 3400 $cm^{-1}$, 2900 $cm^{-1}$, 1430 $cm^{-1}$, and 896 $cm^{-1}$ were the characteristic absorption bands of CNC. This indicated that the internal structure of the CNC did not change during the preparation process. The bands at 3400 $cm^{-1}$ can be attributed to the free O-H stretching vibration of the OH group in the cellulose molecule, and the bands at 2900 $cm^{-1}$ and 1430 $cm^{-1}$ can be attributed to the C-H stretching and bending of the $CH_2$ group. The band at 1640 $cm^{-1}$ was attributable to the bending vibration of the OH group of cellulose, which the presence of this band demonstrates that the cellulose contains adsorbed water (Yang *et al.* 2017; Coelho *et al.* 2018; Xing *et al.* 2018). The peak at 1430 $cm^{-1}$ was attributed to the shear vibration of the hydrogen bond between the C-H molecules in the dehydrated glucopyranose group (Leszczyńska *et al.* 2018). And the peak at 896 $cm^{-1}$ can be attributed to the β-1,4-glycosidic linkage of the glucose unit in the cellulose (Mandal and Chakrabarty 2011; Thomas *et al.* 2015). As shown in Fig. 8, the peak vibration intensity at 896 $cm^{-1}$ was weakened, indicating that the β-glycosidic bond was broken during the hydrolysis, and the size of cellulose was decreased. In the FTIR spectrum, the 1430 $cm^{-1}$ and 896 $cm^{-1}$ bands were considered to be crystalline bands and amorphous bands in cellulose, respectively (Adsul *et al.* 2012; Yang *et al.* 2017; Coelho *et al.* 2018). The crystallinity of cellulose can be estimated from the two peak intensities. The crystallinity of cellulose can be calculated not only by XRD, but also by the following formula (Ciolacu *et al.* 2011; Adsul *et al.* 2012),

$$CrR = A_{1430}/A_{896} \quad (3)$$

$$A = -\log T \quad (4)$$

where $A_{1430}$ represents the absorbance at 1430 $cm^{-1}$, $A_{896}$ represents the absorbance at 896 $cm^{-1}$, and $T$ represents the transmittance.

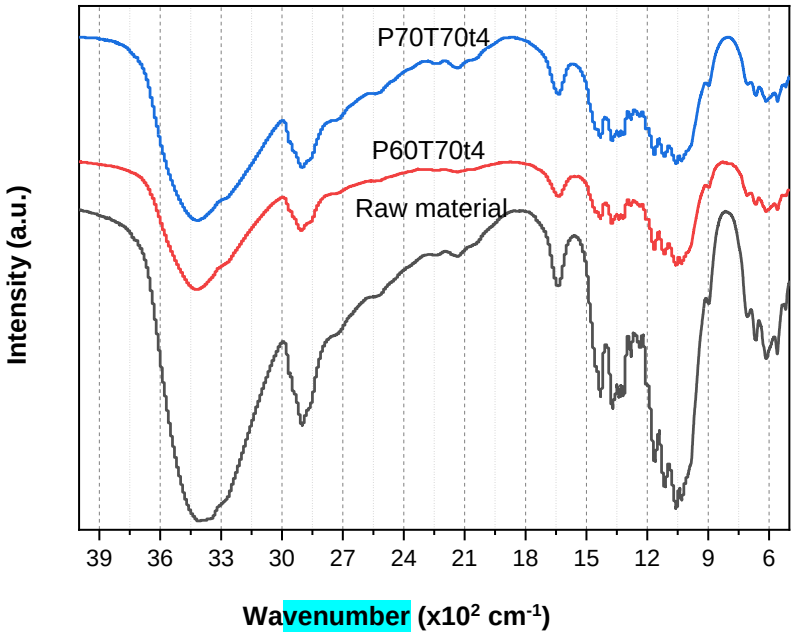


**Fig. 8.** Infrared spectra of CNC prepared under different hydrolysis conditions

The crystallinity of the raw materials and CNC was calculated to be 95.6%, 97.9%, and 98.8%, respectively (Various detection methods were used to calculate the difference in crystallinity, so there was a difference between infrared crystallinity and XRD crystallinity and value.). The trend is consistent with XRD and the XRD results are validated on the trend.

**Table 2.** Peak Intensity of CNC at 1430 $cm^{-1}$ and 896 $cm^{-1}$ under Different Conditions

| | Raw Material | P60T70t4 | P70T70t4 |
|---|---|---|---|
| Transmittance at 1430 $cm^{-1}$ (%) | 71.0 | 84.8 | 91.30 |
| Transmittance at 896 $cm^{-1}$(%) | 86.4 | 93.2 | 96.5 |

In natural cellulose, the hydrogen bond strengths of the two forms of cellulose Iβ and Iα are different, and the position of the O-H band in the infrared spectrum is also different, of which 750 $cm^{-1}$ is attributed to cellulose Iα and 710 $cm^{-1}$ is attributed to cellulose Iβ (Åkerholm *et al.* 2004; Fahma *et al.* 2011; Yu *et al.* 2013). As shown in Fig. 6, the Iβ crystal form characteristic peak appeared in the raw material and the CNC: the OH out-of-plane bending at 710 $cm^{-1}$ (Lu *et al.* 2010, 2013). After acid hydrolysis, it was observed that the peak vibration in the range 1200 $cm^{-1}$ to 1000 $cm^{-1}$ was obviously weakened, among which 1032 $cm^{-1}$ and 1058 $cm^{-1}$ belonged to the C-O-C stretching vibration in the sugar ring (Coelho *et al.* 2018), and 1113 $cm^{-1}$ belonged to the glucose

skeleton vibration. No new functional groups appeared in the spectrogram. It was speculated that during the hydrolysis reaction, the cellulose chain was opened, but no new groups were added. The role of the acid here was only to catalyze the hydrolysis. The peaks at 613 $cm^{-1}$ and 669 $cm^{-1}$ are attributed to the O-H out-of-plane bending vibration, indicating that intermolecular hydrogen bonds interact with each other, resulting in aggregation of CNC (Yu *et al.* 2013), as shown in Figs. 5 and 6.

## X-ray Photoelectron Spectroscopy

The surface properties of cellulose have an important influence on the final properties of the processing and utilization of cellulosic materials (Mitchell *et al.* 2005). XPS has become a new characterization tool for CNC, which was used to analyze the change of cellulose carbon to oxygen ratio and to enable further speculation regarding the possible changes of cellulose groups during degradation. The XPS spectra of the raw materials and the CNC prepared under different conditions are shown in Fig. 9. The two peaks appearing in the XPS spectrum were attributed to the C and O elements in cellulose, and no sulfur was detected. According to the literature, no esterification occurred on the surface of CNC prepared by hydrolysis of p-TsOH (Chen *et al.* 2016). Combined with the infrared spectrum, no ester peak appeared, from which it can be inferred that the surface of the CNC was not connected to the sulfonate group. Therefore, the stability of the suspension of CNC was relatively inferior compared to the introduction of sulfate groups by the sulfuric acid process. The O/C ratio of the cellulose surface was an important indicator of cellulose oxidation (Li *et al.* 2014). As shown in Table 3, the O/C ratio of the CNC was increased by 0.2% after the hydrolysis, which can consider that the cellulose did not oxidize during the hydrolysis.

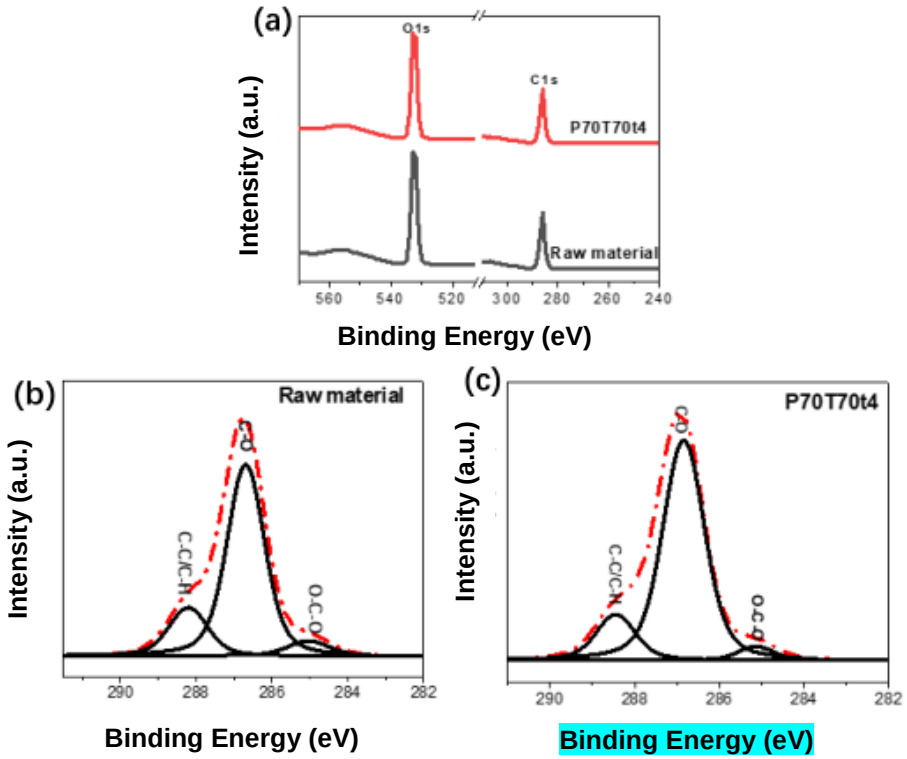


**Fig. 9.** X-ray energy spectrum of raw materials and CNC prepared under different conditions

**Table 3.** O/C Ratio of Raw Materials and CNC of P70T70t4

| | O/C Ratio | Binding Energy | | |
|---|---|---|---|---|
| | | 285.0eV (C-C/C-H) | 286.6eV (C-O) | 288.1ev (O-C-O) |
| Raw material | 0.812 | 0.19 | 0.74 | 0.066 |
| P70T70t4 | 0.814 | 0.15 | 0.80 | 0.05 |

The binding energy spectra of the C1s of the raw materials and the CNC were deconvolved into three Gaussian spectra. The peak positions of these curves were fixed at 285.0 eV, 286.6 eV, and 288.1 eV, representing C-C/C-H, C-O, and O-C-O, respectively (Johansson *et al.* 2005; Mitchell *et al.* 2005; Topalovic *et al.* 2007). Theoretically, the XPS spectrum of cellulose exhibits C1s peaks only at a binding energy of 286.6 eV (C-O, alcohol or ether) and 288.1 eV (O-C-O, diether or carbonyl) with a relative intensity ratio of 5:1, and the C1s expressed at 285.0 eV (C-C/C-H, aliphatic) binding energy are not characteristic of cellulose; rather, they may be derived from lignin, fatty acids, or waxes. (Sapieha *et al.* 1990; Belgacem *et al.* 1995; Mitchell *et al.* 2005; Gray *et al.* 2010). According to Table 3, the value of O/C ratio was lower than the theoretical value of pure cellulose 0.83 (Gray *et al.* 2010). The ratio of C1s at the binding energy of 285 eV decreased from 19% to 15% after hydrolysis, indicating that the non-cellulosic material on the cellulose surface was removed with hydrolysis (p-TsOH can remove lignin efficiently) (Bian *et al.* 2017; Chen *et al.* 2017). The proportion of C1s at the binding energy of 286.6 eV increased, possibly due to acid hydrolysis opening the amorphous region, exposing more alcoholic hydroxyl groups.

## Thermogravimetric Analysis

Results of the thermogravimetric (TG) and derived thermogravimetry (DTG) of CNC obtained under different preparation conditions are shown in Fig. 10 and Table 4. In general, cellulose pyrolysis is divided into two stages, which the first stage is the evaporation of water, the dehydration of cellulose into dehydrogenated cellulose, and the second stage may be related to cellulose depolymerization (Wang *et al.* 2007; Morán *et al.* 2008; Yildirim and Shaler 2017).

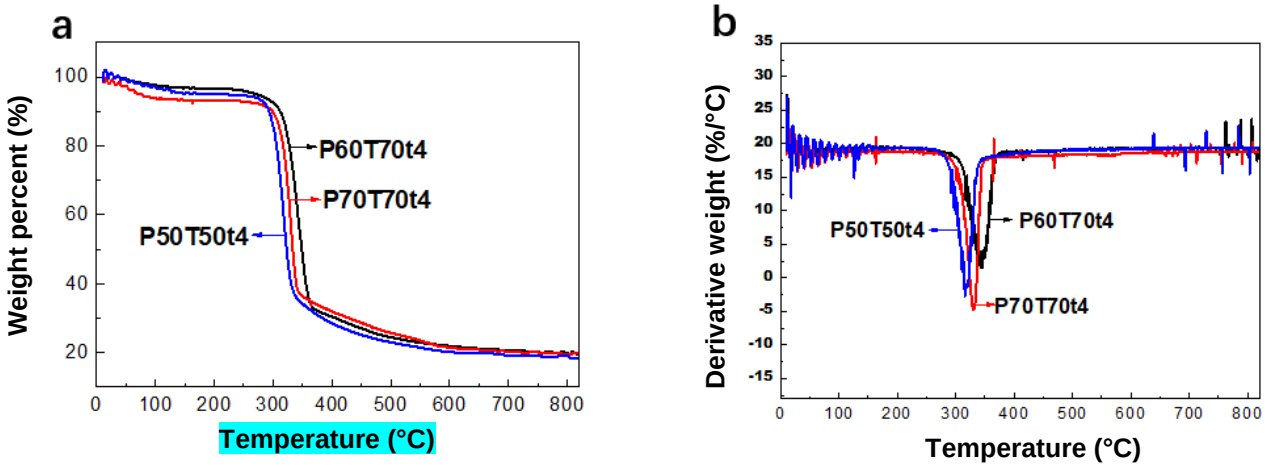


**Fig. 10.** TG and DTG curves of CNC obtained under the treatment of P50T50t4, P60T70t4, and P70T70t4

As shown in the TG curve (Fig. 10a), the free water of the cellulose evaporated near 100 °C, resulting in a small weight loss (about 2.5%) of the CNC. Subsequently, the weight of the CNC began to decrease obviously at about 300 °C, wherein the initial thermal degradation temperature of P50T50t4 was 294 °C, the initial thermal degradation temperature of the CNC of P60T70t4 was 310 °C, and the initial thermal degradation temperature of P70T70t4 was 303 °C. The change in temperature rate here was due to the organic matter starting to decompose at this temperature, and the weight loss was about 60% from 300 °C to 370 °C. Finally, the weight loss of cellulose was slow after about 370 °C, and the carbon residue of P50T50t4, P60T70t4, and P70T70t4 was about 18.9%, 19.8%, 19.5%, respectively, when the temperature reached 800 °C. The increase in carbon residue for the CNC of 70 °C samples in comparison with CNC of 50 °C may be due to small size and increased number of free end chains (Li *et al.* 2012). The DTG curve described the rate of cellulose pyrolysis. The CNC of P50T50t4, P60T70t4, and P70T70t4 reached maximum values at 317 °C, 350 °C, and 331 °C, respectively. Combined with the TG and DTG curves in Fig. 10(a)(b), it was not difficult to find that the CNC obtained by the P60T70t4 condition had the best thermal stability. According to the literature data, the degradation temperature of the CNC obtained by the sulfuric acid method was about 200 °C (Shafizadeh *et al.* 1976; Roman and Winter 2004). Therefore, the thermal stability of CNC obtained by hydrolysis of p-TsOH acid was generally better than that of sulfuric acid method. The reason for this phenomenon may be that the surface of the CNC obtained by the hydrolysis by sulfuric acid introduced sulfate groups, resulting in more heat exposure (Kim *et al.* 2001; Long *et al.* 2017; Nadir and Stephen 2017), while the CNC obtained by hydrolysis of p-TsOH did not introduce new groups on the surface. According to the literature, the introduction of sulfate was the main reason for the low thermal stability (Roman *et al.* 2004).

**Table 4.** Weight Loss and Degradation Temperature of CNC under Different Hydrolysis

| | $T_a$ (°C) | Residue at $T_a$ (%) | $T_b$ (°C) | Residue at $T_b$ (%) | $T_{max}$ (°C) | Residue at 800 °C (%) |
|---|---|---|---|---|---|---|
| P50T50t4 | 112 | 97.2 | 294 | 91.0 | 317 | 18.7 |
| P60T70t4 | 112 | 93.6 | 310 | 90.1 | 350 | 19.8 |
| P70T70t4 | 112 | 96.4 | 303 | 92.2 | 331 | 19.6 |

Note: $T_b$ represents the start of degradation temperature; $T_{max}$ represents the maximum degradation rate.

## CONCLUSIONS

1. The cellulose nanocrystals (CNC) with excellent properties were successfully prepared by hydrolysis of p-toluene sulfonic acid (p-TsOH). It was shown that p-TsOH hydrolysis is a green and highly efficient preparation method, and p-TsOH can be recovered by crystallization, and the recovery rate can reach 71.8%.

2. The CNC were characterized by SEM, TEM, XRD, FTIR, XPS, and TGA. The results showed that the crystallinity index of the CNC with a high aspect ratio (about 33) reached 90%. During the hydrolysis process, no esterification reaction occurred on the surface of the cellulose, and no new groups were introduced on the surface. Therefore, the thermal stability of the CNC was good, and the degradation temperature was about 310 °C. During the hydrolysis process, the crystal form and internal structure of the cellulose were not destroyed.
3. The CNC prepared by hydrolysis of p-TsOH does not introduce new functional groups, and the CNC still has the crystal form and composition of natural cellulose. Therefore, CNC can be used in the fields of electronic components, composite materials, reinforcement materials, and medical materials.

## ACKNOWLEDGMENTS

This research was supported by the Foundation of Key Laboratory of Pulp and Paper Science and Technology of the Ministry of Education (No. KF201706), and by the Shandong Province of China Key Research and Development Project (No. 2019GGX102026) and Shandong Province major innovation project (2018CXGC1001). One of the authors expresses their deepest gratitude to Dr. Songlin Wang who provided valuable guidance during the course of conducting and reporting of this work.

## REFERENCES CITED

Adsul, M., Soni, S. K., Bhargava, S. K., and Bansal, V. (2012). "Facile approach for the dispersion of regenerated cellulose in aqueous system in the form of nanoparticles," *Biomacromolecules* 13(9), 2890-2895. DOI: 10.1021/bm3009022

Åkerholm, M., Hinterstoisser, B., and Salmén, L. (2004). "Characterization of the crystalline structure of cellulose using static and dynamic FT-IR spectroscopy," *Carbohydrate Research* 339(3), 569-578. DOI: 10.1016/j.carres.2003.11.012

Aulin, C., Netrval, J., Wågberg, L., and Lindström, T. (2010). "Aerogels from nanofibrillated cellulose with tunable oleophobicity," *Soft Matter* 6(14), 3298-3305. DOI: 10.1039/c001939a

Belbekhouche, S., Bras, J., Siqueira, G., Chappey, C., Lebrun L., Khelifi B., Marais S., and Dufresne A. (2011). "Water sorption behavior and gas barrier properties of cellulose whiskers and microfibrils films," *Carbohydrate Polymers* 83(4), 1740-1748. DOI: 10.1016/j.carbpol.2010.10.036

Belgacem, M. N., Czeremuszkin, G., Sapieha, S., and Gandini, A. (1995). "Surface characterization of cellulose fibres by XPS and inverse gas chromatography," *Cellulose* 2(3), 145-157. DOI: 10.1007/BF00813015

Bian, H., Chen, L., Dai, H., and Zhu, J. Y. (2017a). "Integrated production of lignin containing cellulose nanocrystals (LCNC) and nanofibrils (LCNF) using an easily recyclable di-carboxylic acid," *Carbohydrate Polymers* 167, 167-176. DOI: 10.1016/j.carbpol.2017.03.050

Bian, H., Chen, L., Gleisner, R., Dai, H., and Zhu, J. Y. (2017b). "Producing wood-based nanomaterials by rapid fractionation of wood at 80 °C using a recyclable acid

hydrotrope," *Green Chemistry* 19(14), 3370-3379. DOI: 10.1039/C7GC00669A

Brinchi, L., Cotana, F., Fortunati, E., and Kenny, J. M. (2013). "Production of nanocrystalline cellulose from lignocellulosic biomass: Technology and applications," *Carbohydrate Polymers* 94(1), 154-169. DOI: 10.1016/j.carbpol.2013.01.033

Carlsson, D. O., Nystršm, G., Ferraz, N., Nyholm, L., Mihranyan, A., and Strømme, M. (2012). "[P1.028] Development of nanocellulose/polypyrrole composites towards blood purification," *Procedia Engineering* 44, 733-736. DOI: 10.1016/j.proeng.2012.08.550

Chang, P. R., Jian, R., Zheng, P., and Yu, J. G. (2010). "Preparation and properties of glycerol plasticized-starch (GPS)/cellulose nanoparticle (CN) composites," *Carbohydrate Polymers* 79(2), 301-305. DOI: 10.1016/j.carbpol.2009.08.007

Chen, L., Dou, J., Ma, Q., Li, N., Wu, R., Bian, H., Yelle, D., Vuorinen, T., Fu, S., Pan, X., and Zhu, J. Y. (2017). "Rapid and near-complete dissolution of wood lignin at ≤ 80°C by a recyclable acid hydrotrope," *Science Advances* 3(9), e1701735. DOI: 10.1126/sciadv.1701735

Chen, L., Wang, Q., Hirth, K., Baez, C., Agarwal, U. P., and Zhu, J. Y. (2015). "Tailoring the yield and characteristics of wood cellulose nanocrystals (CNC) using concentrated acid hydrolysis," *Cellulose* 22(3), 1753-1762. DOI: 10.1007/s10570-015-0615-1

Chen, L., Zhu, J. Y., Baez, C., Kitin, P., and Elder, T. (2016). "Highly thermal-stable and functional cellulose nanocrystals and nanofibrils produced using fully recyclable organic acids," *Green Chem.* 18(13), 3835. DOI: 10.1039/c6gc00687f

Choi, Y. J., and Simonsen, J. (2006). "Cellulose nanocrystal-filled carboxymethyl cellulose nanocomposites," *Journal of Nanoscience and Nanotechnology* 6(3), 633-639. DOI: 10.1166/jnn.2006.132

Ciolacu, D., Ciolacu, F., and Popa, V. I. (2011). "Amorphous cellulose - Structure and characterization," *Cellulose Chemistry and Technology* 45(1), 13-21. DOI: 10.2488/jwrs.57.42

Coelho, D. C. B. K. C., Voorwald, H. J. C., Cioffi, Maria Odila Hilário, Rezende, M. C., and Arantes, V. (2018). "Preparation of nanocellulose from *Imperata brasiliensis* grass using Taguchi method," *Carbohydrate Polymers* 192, 337-346. DOI: 10.1016/j.carbpol.2018.03.055

Dong, H., Snyder, J. F., Tran, D. T., and Leadore, J. L. (2013). "Hydrogel, aerogel, and film of cellulose nanofibrils functionalized with silver nanoparticles," *Carbohydrate Polymers* 95(2), 760-767. DOI: 10.1016/j.carbpol.2013.03.041

Dufresne, A. (2013). "Nanocellulose: A new ageless bionanomaterial," *Materials Today* 16(6), 220-227. DOI: 10.1016/j.mattod.2013.06.004

Elazzouzi-Hafraoui, S., Nishiyama, Y., Putaux, J. L., Heux, L., Dubreuil, F., and Rochas, C. (2008). "The shape and size distribution of crystalline nanoparticles prepared by acid hydrolysis of native cellulose," *Biomacromolecules* 9(1), 57-65. DOI: 10.1021/bm700769p

Fahma, F., Iwamoto, S., Hori, N., Iwata, T., and Takemura, A. (2011). "Effect of pre-acid-hydrolysis treatment on morphology and properties of cellulose nanowhiskers from coconut husk," *Cellulose* 18(2), 443-450. DOI: 10.1007/s10570-010-9480-0

Fernandes, E. M., Pires, R. A., João F. Mano, and Reis, R. L. (2013). "Bionanocomposites from lignocellulosic resources: properties, applications and future trends for their use in the biomedical field," *Progress in Polymer Science*

38(10-11), 1415-1441. DOI: 10.1016/j.progpolymsci.2013.05.013
French, A. D. (2014). "Idealized powder diffraction patterns for cellulose polymorphs," *Cellulose* 21(2), 885-896. DOI: 10.1007/s10570-013-0030-4
Gray, D. G., Weller, M., Ulkem, N., and Lejeune, A. (2010). "Composition of lignocellulosic surfaces: Comments on the interpretation of XPS spectra," *Cellulose* 17(1), 117-124. DOI: 10.1007/s10570-009-9359-0
Guo, X., Liu, L., Hu, Y., and Wu, Y. (2018). "Water vapor sorption properties of tempo oxidized and sulfuric acid treated cellulose nanocrystal films," *Carbohydrate Polymers* 197, 524-530. DOI: 10.1016/j.carbpol.2018.06.0-27
Habibi, Y., Lucia, L. A., and Rojas, O. J. (2010). "Cellulose nanocrystals: Chemistry, self-assembly, and applications," *Chemical Reviews* 110(6), 3479-3500. DOI: 10.1021/cr900339w
Heggset, E. B., Chinga-Carrasco, G., and Syverud, K. (2017). "Temperature stability of nanocellulose dispersions," *Carbohydrate Polymers* 157, 114-121. DOI: 10.1016/j.carbpol.2016.09.077
Herrera, M. A., Mathew, A. P., and Oksman, K. (2014). "Gas permeability and selectivity of cellulose nanocrystals films (layers) deposited by spin coating," *Carbohydrate Polymers* 112, 494-501. DOI: 10.1016/j.carbpol.2014.06.036
Johansson, L. S., Campbell, J. M., Fardim, P., Heijnesson Hultén, A., Boisvert, J. P., and Ernstsson, M. (2005). "An XPS round robin investigation on analysis of wood pulp fibres and filter paper," *Surface Science* 584(1), 126-132. DOI: 10.1016/j.susc.2005.01.062
Karim, Z., Claudpierre, S., Grahn, M., Oksman, K., and Mathew, A. (2016). "Nanocellulose based functional membranes for water cleaning: tailoring of mechanical properties, porosity and metal ion capture," *Journal of Membrane Science* 514, 418-428. DOI: 10.1016/j.memsci.2016.05.018
Kim, D. Y., Nishiyama, Y., Wada, M., and Kuga, S. (2001). "High-yield carbonization of cellulose by sulfuric acid impregnation," *Cellulose* 8(1), 29-33. DOI: 10.1023/a:1016621103245
Leszczyńska, Agnieszka, Radzik, P., Haraźna, K., and Pielichowski, K. (2018). "Thermal stability of cellulose nanocrystals prepared by succinic anhydride assisted hydrolysis," *Thermochimica Acta* 663, 145-156. DOI: 10.1016/j.tca.2018.03.015
Li, W., Yue, J., and Liu, S. (2012). "Preparation of nanocrystalline cellulose via ultrasound and its reinforcement capability for poly(vinyl alcohol) composites," *Ultrasonics Sonochemistry* 19(3), 479-485. DOI: 10.1016/j.ultsonch.2011.11.007
Li, J., Wang, Y., Wei, X., Wang, F., Han, D., Wang, Q., and Kong, L. (2014). "Homogeneous isolation of nanocelluloses by controlling the shearing force and pressure in microenvironment," *Carbohydrate Polymers* 113, 388-393. DOI: 10.1016/j.carbpol.2014.06.085
Lima, M. M. D. S., and Borsali, R. (2004). "Rodlike cellulose microcrystals: structure, properties, and applications," *Macromolecular Rapid Communications* 25(7), 771-787. DOI: 10.1002/marc.200300268
Lin, N., and Dufresne, A. (2014). "Nanocellulose in biomedicine: Current status and future prospect," *European Polymer Journal* 59, 302-325. DOI: 10.1016/j.eurpolymj.2014.07.025
Liu, C., Li, B., Du, H., Lv, D., Zhang, Y., Yu, G., Mu, X., and Peng, H. (2016). "Properties of nanocellulose isolated from corncob residue using sulfuric acid, formic acid, oxidative and mechanical methods," *Carbohydrate Polymers* 151, 716-724.

DOI: 10.1016/j.carbpol.2016.06.025

Liu, P., Borrell, P. F., Božič, M., Kokol, V., Oksman, K., and Mathew, A. P. (2015). "Nanocelluloses and their phosphorylated derivatives for selective adsorption of $Ag^{+}$, $Cu^{2+}$, and $Fe^{3+}$ from industrial effluents," *Journal of Hazardous Materials* 294, 177-185. DOI: 10.1016/j.jhazmat.2015.04.001

Łojewska, J., Missori, M., Lubańska, A., Grimaldi, P., Zięba, K., Proniewicz, L. M., and Congiu Castellano, A. (2007). "Carbonyl groups development on degraded cellulose. correlation between spectroscopic and chemical results," *Applied Physics A* 89(4), 883-887. DOI: 10.1007/s00339-007-4220-5

Long, Y., Yu, Y., Chua, Y. W., and Wu, H. (2017). "Acid-catalysed cellulose pyrolysis at low temperatures," *Fuel* 193, 460-466. DOI: 10.1016/j.fuel.2016.12.067

Lu, P., and Hsieh, Y. L. (2010). "Preparation and properties of cellulose nanocrystals: rods, spheres, and network," *Carbohydrate Polymers* 82(2), 329-336. DOI: 10.1016/j.carbpol.2010.04.073

Lu, Z., Fan, L., Zheng, H., Lu, Q., Liao, Y., and Huang, B. (2013). "Preparation, characterization and optimization of nanocellulose whiskers by simultaneously ultrasonic wave and microwave assisted," *Bioresour. Technol.* 146(10), 82-88. DOI: 10.1016/j.biortech.2013.07.047

Maciel, M. M. Á. D., Benini, K. C. C. C., Voorwald, H. J. C., and Cioffi, M. O. H. (2019). "Obtainment and characterization of nanocellulose from an unwoven industrial textile cotton waste: Effect of acid hydrolysis conditions," *International Journal of Biological Macromolecules* 126(1). 496-506. DOI: 10.1016/j.ijbiomac.2018.12.202.

Mandal, A., and Chakrabarty, D. (2011). "Isolation of nanocellulose from waste sugarcane bagasse (scb) and its characterization," *Carbohydrate Polymers* 86(3), 1291-1299. DOI: 10.1016/j.carbpol.2011.06.030

Martínez-Sanz, M., Lopez-Rubio, A., and Lagaron, J. M. (2011). "Optimization of the nanofabrication by acid hydrolysis of bacterial cellulose nanowhiskers," *Carbohydrate Polymers* 85(1), 228-236. DOI: 10.1016/j.carbpol.2011.02.021

Miettunen, K., Vapaavuori, J., Tiihonen, A., Poskela, A., Lahtinen, P., Halme, J., and Lund, P. (2014). "Nanocellulose aerogel membranes for optimal electrolyte filling in dye solar cells," *Nano. Energy* 8, 95-102. DOI: 10.1016/j.nanoen.2014.05.013

Mirhosseini, H., Tan, C. P., Hamid, N. S. A., and Yusof, S. (2008). "Effect of arabic gum, xanthan gum and orange oil contents on *ζ-potential*, conductivity, stability, size index and pH of orange beverage emulsion," *Colloids & Surfaces A Physicochemical & Engineering Aspects* 315(1-3), 47-56. DOI: 10.1016-/j.colsurfa.2007.07.007

Mishra, R. K., Sabu, A., and Tiwari, S. K. (2018). "Materials chemistry and the futurist eco-friendly applications of nanocellulose: status and prospect," *Journal of Saudi Chemical Society* 22(8), 949-978. DOI: 10.1016/j.jscs.2018.02.005

Mitchell, R., Carr, C. M., Parfitt, M., Vickerman, J. C., and Jones, C. (2005). "Surface chemical analysis of raw cotton fibres and associated materials," *Cellulose* 12(6), 629-639. DOI: 10.1007/s10570-005-9000-9

Morais, J. P. S., Rosa, M. D. F., de Souza Filho, Men de sá Moreira, Nascimento, L. D., Do Nascimento, D. M., and Cassales, A. R. (2013). "Extraction and characterization of nanocellulose structures from raw cotton linter," *Carbohydrate Polymers* 91(1), 229-235. DOI: 10.1016/j.carbpol.2012.08.010

Morán, J. I., Alvarez, V. A., Cyras, V. P., and Vázquez, A. (2008). "Extraction of cellulose and preparation of nanocellulose from sisal fibers," *Cellulose* 15(1), 149.

DOI: 10.1007/s10570-007-9145-9
Mounika, M., and Ravindra, K. (2015). "Characterization of nanocomposites reinforced with cellulose whiskers: a review," *Materials Today: Proceedings* 2(4-5), 3610-3618. DOI: 10.1016/j.matpr.2015.07.107
Nadir, Y., and Stephen, S. (2017). "A study on thermal and nanomechanical performance of cellulose nanomaterials (CNs)," *Materials* 10(7), 718, DOI: 10.3390/ma10070718
Nair, S. S., Zhu, J. Y., Deng, Y., and Ragauskas, A. J. (2014). "High performance green barriers based on nanocellulose," *Sustainable Chemical Processes* 2(1), 23. DOI: 10.1186/s40508-014-0023-0
Oksman, K., Yvonne Aitomäki, Mathew, A. P., Siqueira, G., Zhou, Q., Butylina, S., Tanpichai, S., Zhou, X., and Hooshmand, S. (2016). "Review of the recent developments in cellulose nanocomposite processing," *Composites Part A: Applied Science & Manufacturing* 83, 2-18. DOI: 10.1016/j.compositesa.2015.1-0.041
Orts, W. J., Shey, J., Imam, S. H., Glenn, G. M., Guttman, M. E., and Revol, J. F. (2005). "Application of cellulose microfibrils in polymer nanocomposites," *Journal of Polymers and the Environment* 13(4), 301-306. DOI: 10.1007/s10924-005-5514-3
Pereira, André Luís S., Nascimento, D. M. D., Souza Filho, Men de sá M., Morais, J. P. S., Vasconcelos, N. F., Feitosa, J. P. A., Brígida, Ana Iraidy S., Rosa, and Morsyleide de F. (2014). "Improvement of polyvinyl alcohol properties by adding nanocrystalline cellulose isolated from banana pseudostems," *Carbohydrate Polymers* 112, 165-172. DOI: 10.1016/j.carbpol.2014.05.090
Roman, M., and Winter, W. T. (2004). "Effect of sulfate groups from sulfuric acid hydrolysis on the thermal degradation behavior of bacterial cellulose," *Biomacromolecules* 5(5), 1671-1677. DOI: 10.1021/bm034519+
Samir, M. A., Alloin, F., and Dufresne, A. (2005). "Review of recent research into cellulosic whiskers, their properties and their application in nanocomposites field," *Biomacromolecules* 6(2), 612-626. DOI: 10.1021/bm0493685
Santos, F. A. D., Iulianelli, G. C. V., and Maria Inês Bruno Tavares. (2016). "The use of cellulose nanofillers in obtaining polymer nanocomposites: Properties, processing, and applications," *Materials Sciences & Applications* 07(5):257-294. DOI: 10.4236/msa.2016.75026
Sapieha, S., Verreault, M., Klemberg-Sapieha, J. E., Sacher, E., and Wertheimer, M. R. (1990). "X-ray photoelectron study of the plasma fluorination of lignocellulose," *Applied Surface Science* 44(2), 165-169. DOI: 10.1016/0169-4332(90)90105-9
Seabra, A. B., Bernardes, J. S., Wagner J. Fávaro, Paula, A. J., and Nelson Durán. (2017). "Cellulose nanocrystals as carriers in medicine and their toxicities: a review," *Carbohydrate Polymers* 181, 514. DOI: 10.1016/j.carbpol.2017.12.014
Segal, L., Creely, J. J., Martin, A. E., and Conrad, C. M. (1959). "An empirical method for estimating the degree of crystallinity of native cellulose using the X-ray diffractometer," *Text. Res. J.* 29(10), 786-794. DOI: 10.1177/0040517559029-01003
Shafizadeh, F., Sarkanen, K. V., and Tillman, D. A. (1976). "Thermal uses and properties of carbohydrates and lignins," *Thermal Uses & Properties of Carbohydrates & Lignins* 99(10), 317-320. DOI: 10.1002/bjs.8876
Sol, V. (2016). "Development of curcumin-cyclodextrin/cellulose nanocrystals complexes: new anticancer drug delivery systems," *Bioorganic & Medicinal Chemistry Letters* 26(3), 941-945. DOI: 10.1016/j.bmcl.2015.12.060
Stelte, W., and Sanadi, A. R. (2009). "Preparation and characterization of cellulose nanofibers from two commercial hardwood and softwood pulps," *Industrial &*

*Engineering Chemistry Research* 48(24), 11211-11219. DOI: 10.1021/ie9011672

Teixeira, R. S. S., Silva, Ayla Sant'Ana da, Jang, J. H., Kim, H. W., Ishikawa, K., Endo, T., Seung-HwanLee, and Elba P. S. Bon. (2015). "Combining biomass wet disk milling and endoglucanase/β-glucosidase hydrolysis for the production of cellulose nanocrystals," *Carbohydrate Polymers* 128, 75-81. DOI: 10.1016/j.carbpol.2015.03.087

Theivasanthi, T., Anne, F. C., Toyin, A. J., Gopinath, S., and Ravichandran, R. (2018). "Synthesis and characterization of cotton fiber-based nanocellulose," *International Journal of Biological Macromolecules* 109. DOI: 10.1016/j.ijbio-mac.2017.11.054

Thomas, M. G., Abraham, E., Jyotishkumar, P., Pothan, L. A., Maria, H. J., and Thomas, S. (2015). "Nanocelluloses from jute fibres and their nanocomposites with natural rubber: preparation and characterization," *International Journal of Biological Macromolecules* 81, 768-777. DOI: 10.1016/j.ijbiomac.2015.08.053

Tian, C., Yi, J., Wu, Y., Wu, Q., Qing, Y., and Wang, L. (2016). "Preparation of highly charged cellulose nanofibrils using high-pressure homogenization coupled with strong acid hydrolysis pretreatments," *Carbohydrate Polymers* 136, 485-492. DOI: 10.1016/j.carbpol.2015.09.055

Tingaut, P., Zimmermann, T., and Sèbe, Gilles. (2012). "Cellulose nanocrystals and microfibrillated cellulose as building blocks for the design of hierarchical functional materials," *Journal of Materials Chemistry* 22(38), 20105. DOI: 10.1039/c2jm32956e

Topalovic, T., Nierstrasz, V. A., Bautista, L., Jocic, D., Navarro, A., and Warmoeskerken, M. M. C. G. (2007). "XPS and contact angle study of cotton surface oxidation by catalytic bleaching," *Colloids and Surfaces A (Physicochemical and Engineering Aspects)* 296(1-3), 76-85. DOI: 10.1016/j.colsurfa.2006.09.026

Wang, N., Ding, E., and Cheng, R. (2007). "Thermal degradation behaviors of spherical cellulose nanocrystals with sulfate groups," *Polymer* 48(12), 3486-3493. DOI: 10.1016/j.polymer.2007.03.062

Xing, J., Tao, P., Wu, Z., Xing, C., Liao, X., and Nie, S. (2018). "Nanocellulose-graphene composites: A promising nanomaterial for flexible supercapacitors," *Carbohydrate Polymers* 207, 447-459. DOI: 10.1016/j.carbpol.2018.12.010

Xing, L., Gu, J., Zhang, W., Tu, D., and Hu, C. (2018). "Cellulose I and II nanocrystals produced by sulfuric acid hydrolysis of Tetra-pak cellulose I," *Carbohydrate Polymers* 192, 184-192. DOI: 10.1016/j.carbpol.2018.03.042

Xu, X., Liu, F., Jiang, L., Zhu, J. Y., Haagenson, D., and Wiesenborn, D. P. (2013). "Cellulose nanocrystals vs. cellulose nanofibrils: A comparative study on their microstructures and effects as polymer reinforcing agents," *ACS Applied Materials & Interfaces* 5(8), 2999-3009. DOI: 10.1021/am302624t

Yang, X., Han, F., Xu, C., Jiang, S., Huang, L., Liu, L., and Xia, Z. (2017). "Effects of preparation methods on the morphology and properties of nanocellulose (NC) extracted from corn husk," *Industrial Crops and Products* 109, 241-247. DOI: 10.1016/j.indcrop.2017.08.032

Yatagai, M., and Zeronian, S. H. (1994). "Effect of ultraviolet light and heat on the properties of cotton cellulose," *Cellulose* 1(3), 205-214. DOI: 10.1007/BF0081-3508

Yildirim, N., and Shaler, S. (2017). "A study on thermal and nanomechanical performance of cellulose nanomaterials (CNs)," *Materials* 10(7), 718. DOI: 10.3390/ma10070718

Yu, H., Qin, Z., Liang, B., Liu, N., Zhou, Z., and Chen, L. (2013). "Facile extraction of thermally stable cellulose nanocrystals with a high yield of 93% through hydrochloric

acid hydrolysis under hydrothermal conditions," *Journal of Materials Chemistry A*, 1, 3938. DOI: 10.1039/C3TA01150J

Zhang, T., Zhang, Y., Wang, X., Liu, S., and Yao, Y. (2018). "Characterization of the nano-cellulose aerogel from mixing CNF and CNC with different ratio," *Materials Letters* 229, 103-106. DOI: 10.1016/j.matlet.2018.0-6.101

Zu, G., Shen, J., Zou, L., Wang, F., and Zhang, Y. (2015). "Nanocellulose-derived highly porous carbon aerogels for supercapacitors," *Carbon* 99, 203-211. DOI: 10.1016/j.carbon.2015.11.079

Article submitted: June 28, 2019; Peer review completed: August 26, 2019; Revised version received: September 12, 2019; Accepted: September 27, 2019; Published: October 10, 2019.
DOI: 10.15376/biores.14.4.9331-9351